Potential of thorium molten salt reactors: detailed calculations and concept evolution with a view to large scale energy production

A. Nuttin, D. Heuer, A. Billebaud, R. Brissot, C. Le Brun, E. Liatard, J.M. Loiseaux, L. Mathieu, O. Meplan, E. Merle-Lucotte, et al.

POTENTIAL OF THORIUM MOLTEN SALT REACTORS : DETAILED CALCULATIONS AND CONCEPT EVOLUTIONS IN VIEW OF A LARGE NUCLEAR ENERGY PRODUCTION

A. NUTTIN, D. HEUER, A. BILLEBAUD, R. BRISSOT,
C. LE BRUN, E. LIATARD, J.-M. LOISEAUX, L. MATHIEU,
O. MEPLAN, E. MERLE-LUCOTTE, H. NIFENECKER, F. PERDU

Laboratoire de Physique Subatomique et de Cosmologie
CNRS/IN2P3 - UJF - ENSPG, 38026 Grenoble cedex, France

S. DAVID

Institut de Physique Nucléaire d'Orsay
CNRS/IN2P3 - UPS, 91406 Orsay cedex, France

Abstract

We discuss here the concept of Thorium Molten Salt Reactor dedicated to future nuclear energy production. The fuel of such reactors being liquid, it can be easily reprocessed to overcome neutronic limits. In the late sixties, the MSBR project showed that breeding is possible with thorium in a thermal spectrum, provided that an efficient pyrochemical reprocessing is added. With tools developed around the Monte Carlo MCNP code, we first re-evaluate the performance of a MSBR-like reference system with ^{232}Th/^{233}U fuel. We find an important reduction of inventories and induced radiotoxicities at equilibrium compared to other fuel cycles, with a doubling time of about thirty years.

We then study how to start this interesting reference system with the plutonium from PWR spent fuel. Such a transition appears slow and difficult, since it is very sensitive to the fissile quality of the plutonium used. Deployment scenarios of ^{232}Th/^{233}U MSBR-like systems from the existing French PWRs demonstrate the advantage of an upstream ^{233}U production in other reactors, allowing a direct start of the MSBR-like systems with ^{233}U. This finally leads us to explore alternatives to some MSBR features, for energy production with ^{232}Th/^{233}U fuel from the start. We thus test different options, especially in terms of core neutronics optimization and reprocessing unit adaptation.

Keywords

thorium fuel, Molten Salt Reactor, MCNP, radiotoxicity, pyrochemistry

1. INTRODUCTION

Nuclear energy, as it is today, is at the center of political debates mainly because of the waste it produces. About two thirds of the nuclear power being produced in the world rest on Pressurized Water Reactors (PWRs), using a ^{235}U-enriched uranium fuel. This type of fuel leads to a significant production of plutonium and, to a lower extent, of minor actinides, i.e. neptunium, americium and curium. If stored in geological depositories, plutonium would dominate waste radiotoxicity in the long term. In fact, only if nuclear power is a small or vanishing contributor to the total energy supply can plutonium really be considered as a waste. Already in French PWRs, plutonium is being partially recycled once in a so-called MOX fuel. As a result, its piling up is slowed down. Many studies are being carried out on geological storage and on incineration in subcritical reactors, in order to optimize the solutions to the back-end problems. It is also necessary to evaluate other possible nuclear fuel cycles, like the thorium cycle described by the following process :

$$^{232}\mathrm{Th} + \mathrm{n} \longrightarrow {}^{233}\mathrm{Th} \xrightarrow{\beta^- \ (22.3\ \mathrm{min})} {}^{233}\mathrm{Pa} \xrightarrow{\beta^- \ (27\ \mathrm{d})} {}^{233}\mathrm{U} \tag{1}$$

This fuel cycle leads to a reduced waste production. We discuss it here as an alternative form of nuclear energy in the case of a significant contribution to the world energy supply. During the past thirty years, the total primary energy consumption has grown from 6.0 to 9.7 Gtep, with a 7%-decrease of the fossil fuel share (79.2% in 1999) in favour of nuclear (6.8%) and renewable (0.6%) sources. Such an evolution could be accelerated over the next decades, because of new ecological constraints such as the already observed increase of the world mean temperature called "global warming". Today there is a strong consensus that anthropic CO_2 emissions from fossil fuels represent the main contribution to this effect. International conferences have therefore tried to limit the use of fossil fuels, but even the stabilization of CO_2 emissions required in 1997 by the well-known Kyoto protocol seems out of reach. A significant drop of the fossil fuel share could be all the more necessary as reserves are limited (40 years for petrol and 60 years for gas, at the present consumption rate), while the total energy consumption is expected to double by 2050. Most scenarios take this necessity into account, with various types of share evolution for the alternative energy sources [1].

Some "nuclear intensive" scenarios consider a more than 30% increase of the nuclear share in the primary energy production by 2050, that is to say more than a factor of 10 on the currently installed power [2]. Nuclear energy would then have to fulfill a few essential requirements for a sustainable development. In other words, it would have to be as economical, clean and safe as possible. Preserving natural resources imposes fissile regeneration by capture on a fertile support of thorium or uranium. If the neutron margin available after fissile regeneration is greater than the parasitic capture rate, extra fissile matter is bred and can be used to start new reactors. Breeding ^{239}Pu from ^{238}U is easy but requires fast neutrons, whereas breeding ^{233}U from ^{232}Th is slightly feasible with either thermal or fast neutrons. Fuel cycles based on uranium in a thermal spectrum cannot be considered sustainable. The second constraint, that of cleanliness, deals with the minimization of ultimate wastes. Thorium fuels produce much less plutonium and minor actinides than uranium fuels, so that induced radiotoxicities are lower by more than two orders of magnitude [3]. Comparative studies on the thorium cycle show that the fissile inventory can be reduced by almost a factor of 10 with thermal neutrons as compared to fast neutrons, thanks to more favorable cross section values in the regenerating mode [4]. With equivalent reprocessing losses, this lower inventory simply implies less waste and, thus, lower induced radiotoxicities. For all these reasons, thorium with thermal neutrons is a very promising option for scenarios with a significant nuclear contribution. The aim of this paper is to evaluate precisely the potential of this option in terms of breeding, waste production and, last but not least, safety, when associated to the well-adapted concept of Molten Salt Reactor (MSR).

2. GENERAL PRESENTATION OF A REFERENCE MOLTEN SALT BREEDER REACTOR

2.1. Brief historical review of experiments and studies

The MSR concept was first studied in the fifties at the Oak Ridge National Laboratory (ORNL), with the Aircraft Reactor Experiment of a reactor for plane based on a liquid uranium fluoride fuel circulating in a BeO moderator. Studies were then oriented on a civilian application of this concept to electricity production. The Molten Salt Reactor Experiment (MSRE) managed from 1964 to 1969 the operation of a 8 MWth graphite-moderated MSR, with a liquid fuel made of lithium and beryllium fluorides. A third component of the salt was first enriched uranium, then ^{233}U and finally plutonium fluoride [5]. The main results of the MSRE are materials improvement against corrosion, control of reactivity and understanding of fuel behaviour. Its success led to the Molten Salt Breeder Reactor (MSBR) project of a 1 GWe industrial reactor based on the thorium cycle [6]. Figure 1 sketches the full system, including a graphite-moderated core with channels for LiF-BeF_2-ThF_4 fuel circulation and a pyrochemical reprocessing unit. The latter extracts most capturing Fission Products (FPs), which is essential for ^{233}U breeding with the MSBR thermal spectrum. Another feature is the temporary storage of the extracted protactinium, in order to let ^{233}Pa decay out of flux into ^{233}U. The doubling time was evaluated to about 25 years, for a ^{233}U inventory of about one (metric) ton.

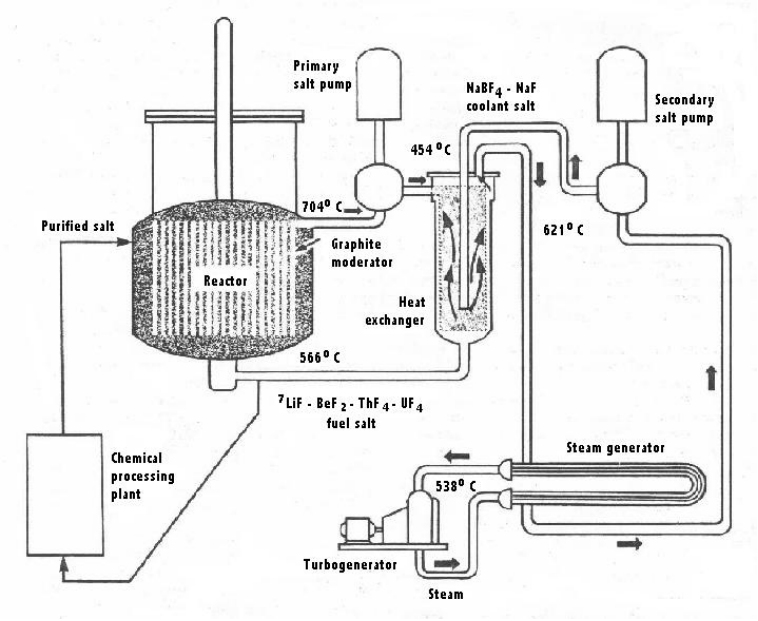

Figure 1: Global description of the MSBR project.

The MSBR project was stopped at Oak Ridge in 1976. It was then re-evaluated in France until the early 80's [7]. The Japanese program Thorims-NES later proposed to separate ^{233}U production from energy production in a simplified MSR with thorium support [8]. In the past few years, the Thorium Molten Salt Reactor (TMSR) concept for energy production with thorium has been studied again in France, with the idea to explore all its potentialities and to simplify it consequently [9][10]. It is one of the six systems selected by the Generation IV International Forum on future reactors [11].

2.2. Use of molten salts as fuel salts in nuclear reactors

Commonly used in the chemical industry, both chloride and fluoride molten salts have many interesting features. But the choice of a fuel salt has to proceed from a compromise between its physico-chemical properties and neutronic constraints such as parasitic absorption.

Molten salts have low fusion temperatures, high heat capacity and medium heat conductivity, that is to say good coolant properties. Nuclear damages do not exist, and chemical inertness with water and air is high. Nevertheless, corrosion at high temperatures necessitates resistant materials, such as the Hastelloy-N steel developed at Oak Ridge during the MSRE. In most cases and in particular for the graphite-moderated TMSR, fluorides are better than chlorides since they are less corrosive and more transparent to neutrons. Their melting points are higher than those of chlorides, but can be sufficiently reduced by the use of a third component like in the so-called "FLiBe" salt chosen for the MSBR with a melting point of 500 ^{o}C. Its molar composition is 72% LiF - 16% BeF_2 - 12% ThF_4, with a density of 3.3 g/cm^3 at the mean operating temperature of 650 ^{o}C.

2.3. Description of MSBR online pyrochemical reprocessing

Pyrochemistry has been widely studied for its applications to spent fuel reprocessing, with at least three possible processes : precipitation, electrorefining and reductive extraction. We focus here on the latter process, which consists in extracting elements from their salt phase into a countercurrent reductive liquid metal. In the MSBR project, the continuous reprocessing aims at the reductive extraction of MF_n rare earth fluorides from the fuel salt into liquid bismuth :

$$MF_n \ + \ n \ Li_{(Bi)} \ \rightleftharpoons \ M_{(Bi)} \ + \ n \ LiF \tag{2}$$

The equilibrium constant of Reaction 2 determines the distribution of M between the salt and the metal in function of the Li distribution. Because actinides are the elements most easily extracted from the salt in the FLiBe/Bi system, the MSBR reprocessing unit carries out their reductive extraction first. The extracted actinides are temporarily stored, before being re-injected as detailed in the flow diagram of Figure 2. By means of a higher Li molar fraction in Bi, a second reductive extraction step proceeds then to lanthanide extraction while leaving most of the residual actinides in the salt [12].

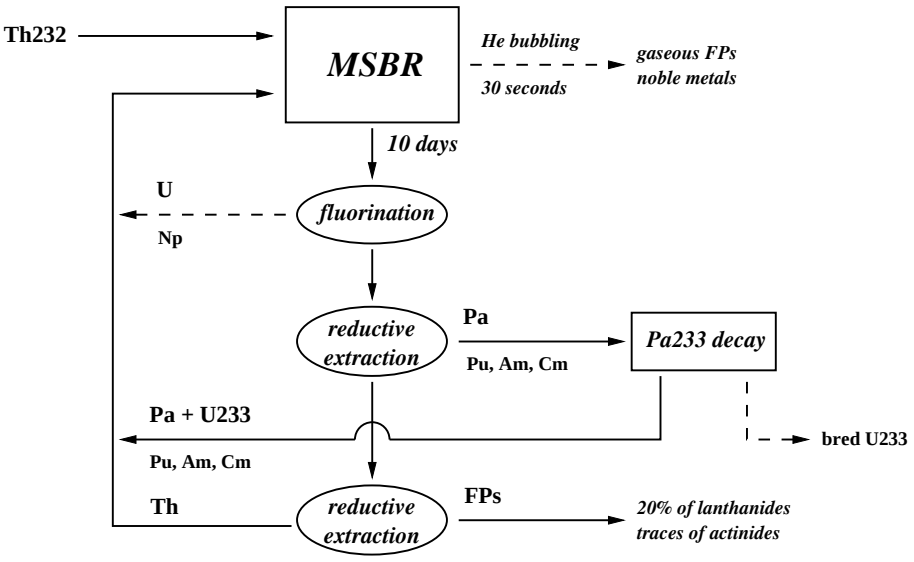

Figure 2: Simplified flow diagram of the MSBR reprocessing unit.

Additional reprocessing and maintenance operations are done on the fuel salt, they are summarized in Figure 2. A preliminary fluorination allows to extract and quickly reinject uranium in the core before actinide extraction, in order to minimize fissile inventory and losses. Protactinium is then extracted from the salt with other actinides, and stored a few months to let ^{233}Pa entirely decay into ^{233}U. The amount of ^{233}U bred in excess is not reinjected, it is set aside to start new reactors.

3. PRINCIPLES OF COMPUTING TOOLS DEVELOPED FOR REACTOR SIMULATIONS

3.1. About the Monte Carlo MCNP code

All our neutronic calculations were done with the MCNP code [13], which allows to follow neutron propagation in reactor cores. For each neutron followed, this code computes the mean free path and deduces the length travelled by using a random number generator. Then, the reaction and its products are determined according to probability tables built from nuclear data files. In each geometric cell part of the total simulated system, the mean cross section σ of any nuclear reaction is defined by :

$$\sigma = \frac{\int_E \int_{\overrightarrow{r}} \sigma(E)\phi(E, \overrightarrow{r})dEd^3\overrightarrow{r}}{\int_E \int_{\overrightarrow{r}} \phi(E, \overrightarrow{r})dEd^3\overrightarrow{r}} \tag{3}$$

The average flux ϕ in the volume V of such a cell is given by Formula 4. The global average value of the flux in a group of MCNP cells is given by the sum of the average fluxes in these cells, weighted by the respective volumes. For cross sections, the sum is weighted by the respective $\phi.V$ factors.

$$\phi = \frac{1}{V} \int_E \int_{\overrightarrow{r}} \phi(E, \overrightarrow{r})dEd^3\overrightarrow{r} \tag{4}$$

Using the MCNP code for cross section and flux calculations thus implies a detailed geometrical description of the system, in order to have precise results without too long runs. It necessitates also to exploit the most recent and complete nuclear data available. With the σ and ϕ static values obtained from MCNP, it is then possible to compute the time evolution of the system.

3.2. Coupling MCNP to an evolution program

During the operation of a reactor, most of its physical parameters are evolving. To take this evolution into account, we developed a program which chains successive MCNP calculations for an optimal update of neutronic values. The goal of this program is the resolution of the so-called Bateman differential equations in each cell composing the geometry, resulting in the time evolution of isotopic compositions and of every other parameter of the system being simulated. We break up the evolution calculation into three levels of time steps, as shown in Figure 3. The first level aims at minimizing the number of MCNP runs, according to a user-defined precision, by trying to progressively increase the length of MCNP steps during the transition to salt complete equilibrium. For a smoother evolution, all mean cross sections are interpolated by a third degree function between MCNP values.

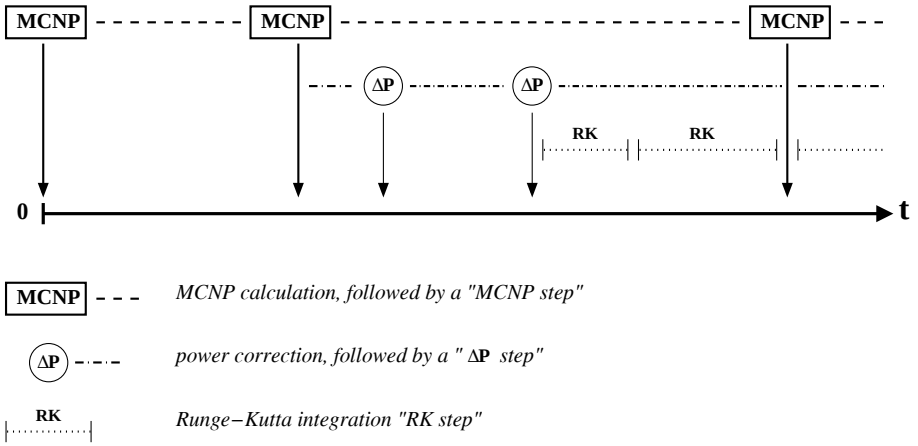

Figure 3: Representation of the three levels of an evolution calculation.

The second level aims at checking that the total power has not changed during the current step by more than an user-defined limit. If this happens because of mean cross section evolution, the flux renormalization factor, which corresponds to the total number of MCNP source neutrons per second, is recalculated in order to fulfill the condition of constant power. This operation is equivalent, in a critical reactor, to the tuning of the flux by the position of control rods. At these power correction times, an evaluation of k_{eff}, which can be used for online control, is obtained from reaction rates and neutron leakage values. The third and last level deals with the numerical integration itself for each evolution cell, by means of a fourth order Runge-Kutta variable step method. Step lengths depend on cells and required precisions, but all are synchronized with the power correction times.

3.3. Optimal exploitation of nuclear and chemical data

In addition to the integration driven by precision requirements, we interfaced a preparation step for the writing of the appropriate MCNP input file. Other parts of our computing tools, globally summarized in Figure 4, deal with the management of basic nuclear and chemical data.

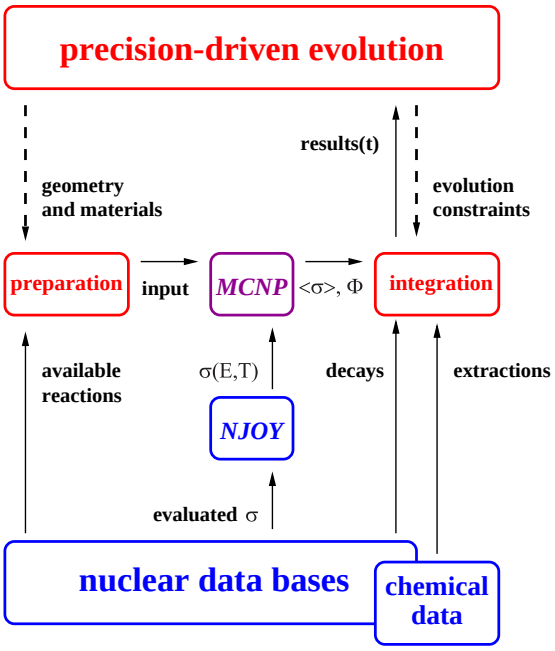

Figure 4: Organization of evolution tools around MCNP.

An "evolution tree" of nuclei is built for each cell at the very beginning, taking into account every reaction and decay present in the data bases. We choose ENDF/B-VI, JENDL 3.2 and JEF 2.2 as priority order. Nuclei whose half-life is below a threshold set to 10 hours are short-circuited and their data are no longer needed. The nuclear data processing NJOY code [14] builds the file for MCNP of any new nucleus at the appropriate temperature, to take the Doppler effect into account.

In the MSBR project, the entire salt is reprocessed within a time T_r of 10 days. The amount dN_e of element e with inventory N_e extracted during dt is proportional to the quantity $N_e \times \frac{dt}{T_r}$ submitted to extraction, with extraction efficiency ε_e. Formula 5 shows that extraction amounts to a fictive decay of time constant $\lambda_e = \frac{\varepsilon_e}{T_r}$. Chemical data are taken into account likewise in the evolution. For gaseous FPs (Xe, Kr) and noble metals (Tc) quickly extracted by He bubbling, $\frac{1}{\lambda_e}$ is set to 30 s.

$$dN_e = N_e \frac{dt}{T_r} \varepsilon_e \tag{5}$$

4.1. Definition at start-up

Let us first describe the reactor geometry that we keep in this section, resulting from neutronic preliminary studies. Materials have to be defined precisely. In order to make comparisons with former simulations, we choose graphite with the maximal density of 2.3 g/cm^3. We choose a fuel salt similar to the MSBR FLiBe : LiF-BeF_2-(Th/U)F_4 at 70-17.5-12.5 mol% respectively, with the same density of 3.3 g/cm^3 at 900 K. Lithium is ^{7}Li at 99.995 mol% in order to minimize ^{6}Li capture.

The quarter vertical section drawn to scale in Figure 5 shows our geometrical modelization of the reactor. The core is a cylindrical assembly (2.3 m radius, 4.6 m high) of graphite hexagons (15 cm side), each pierced by a channel (15 cm diameter) for salt circulation. Around this core, the 50 cm thick graphite radial reflector maximizes the value of k_{eff}, together with the 1.3 m high axial reflectors. The fuel salt circuit (46.2 m^3) is broken up into three MCNP cells : one for the salt channels (20.5 m^3), one for the two 30 cm high salt plena above and below the core (10.3 m^3) and the last one for the heat exchangers (15.4 m^3), protected by a 10 cm thick layer of B_4C.

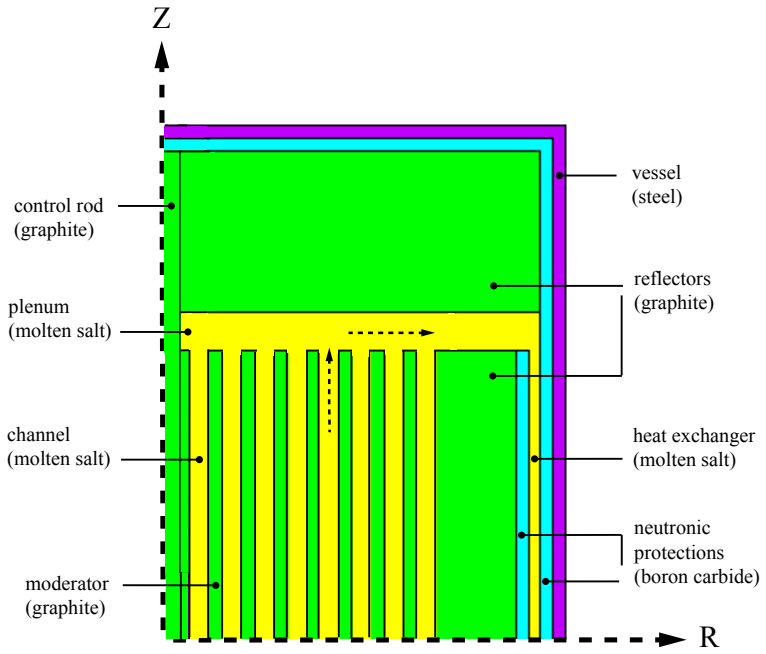

Figure 5: Geometrical description of the core for MCNP.

Let us check that the initial conditions allow optimal ^{233}U breeding at the fixed operating power of 2500 MWth. Table 1 shows that the flux is lower by one order of magnitude in the plena as compared to the channels, and likewise in the exchangers as compared to the plena. The breeding ratio, obtained by dividing the total ^{232}Th capture rate $\tau_{cap}^{^{232}Th}$ by the total ^{233}U absorption rate $\tau_{abs}^{^{233}U}$, indicates a net ^{233}U production at start-up. The neutron spectrum is epithermal, with a graphite contribution to the mean lethargy gain close to 90%. In order to adjust k_{eff} to 1, the ^{233}U concentration in the initial heavy nuclei load is set to 1.6 mol%, which amounts to an inventory of 1.1 tons of ^{233}U for 67 tons of ^{232}Th. The maximal volumic power in the salt is 200 W/cm^3, for an average value of 120 W/cm^3, giving a shape factor of 1.7. Heat extraction imposes that the salt flow velocities range from 0.7 m/s at the edge to 2.0 m/s at the center, which is consistent with the 0.6-2.4 m/s MSBR range [6].

	channels	salt plena	exchangers	total circuit
$N^{^{232}Th}$ (mol)	1.28 10^5	6.4 10^4	9.6 10^4	2.88 10^5
$\sigma^{^{232}Th}_{capture}$ (barn)	1.62	1.25	1.23	1.60
$\tau^{^{232}Th}_{cap}$ (mol/day)	12.97	0.52	0.05	**13.54**
$N^{^{233}U}$ (mol)	2.13 10^3	1.07 10^3	1.60 10^3	4.80 10^3
$\sigma^{^{233}U}_{fission}$ (barn)	80.9	35.9	43.6	78.4
$\sigma^{^{233}U}_{capture}$ (barn)	9.9	4.8	5.2	9.58
$\tau^{^{233}U}_{abs}$ (mol/day)	12.10	0.28	0.03	**12.41**
ϕ (n.cm^{-2}.s^{-1})	7.24 10^{14}	0.75 10^{14}	0.05 10^{14}	3.40 10^{14}
breeding ratio	1.07	1.86	1.67	**1.09**

Table 1: Initial inventories N and mean cross sections σ of ^{232}Th and ^{233}U in the LiF-BeF_2-(Th/U)F_4 fuel salt, detailed cell by cell for the calculation of the global breeding ratio.

In all our simulations, the reactor is kept critical from its start-up to its complete equilibrium within an MCNP uncertainty margin of about 200 pcm. While respecting this criticality condition, we checked that the reference system was optimal for ^{233}U breeding as regards the molar proportion of actinides in the salt (12.5%) and the volumic proportion of salt in the core (30.2%).

4.2. Transition to equilibrium

We coupled a reprocessing model to the MCNP geometry, according to the MSBR pyrochemical operations described in Figure 2. As mentioned in Subsection 3.3, we assume that rare gases like xenon escape with flowing helium in less than one minute, together with noble metals. Soluble Fission Products are classified in three categories with extraction efficiencies of 20% (rare earths and halogens), 5% (semi-noble metals) and 1% (alkaline elements). We assume that protactinium is extracted with 100% efficiency within the reprocessing time T_r of 10 days. The actinide loss rate is taken equal to 10^{-5} over these 10 days, so that it amounts to the case of a solid fuel reprocessed every 5 years with present separation performance. The efficiency of the uranium fluorination preliminary step is set to 99%, leading to an uranium global loss rate of 10^{-7} over $T_r = 10$ days.

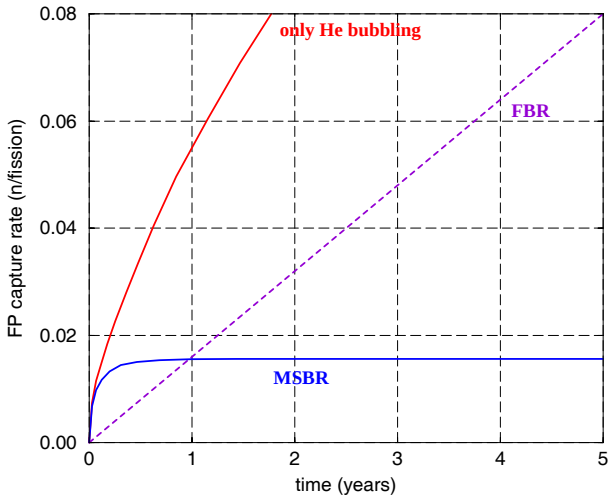

Figure 6: Evolution of FP capture rate (in n/fission) in our MSBR-like system, compared to the case without FP extraction (only He bubbling) and to the case of a solid fuel Fast Breeder Reactor [3].

A first result of the calculation is the quick stabilization of the FP capture rate, at a sufficiently low level to allow breeding. It takes FPs about 5 years to reach their equilibrium inventory of 210 kg, while their mean cross section decreases during the first months from about 25 to 3.2 barns. Figure 6 represents the evolution of the FP capture rate, normalized to one fission. In our reference MSBR-like system, this rate stabilizes in a few months to less than half the value of a FBR averaged over its 5-year operation period. Without soluble FP extraction, helium bubbling is clearly not sufficient.

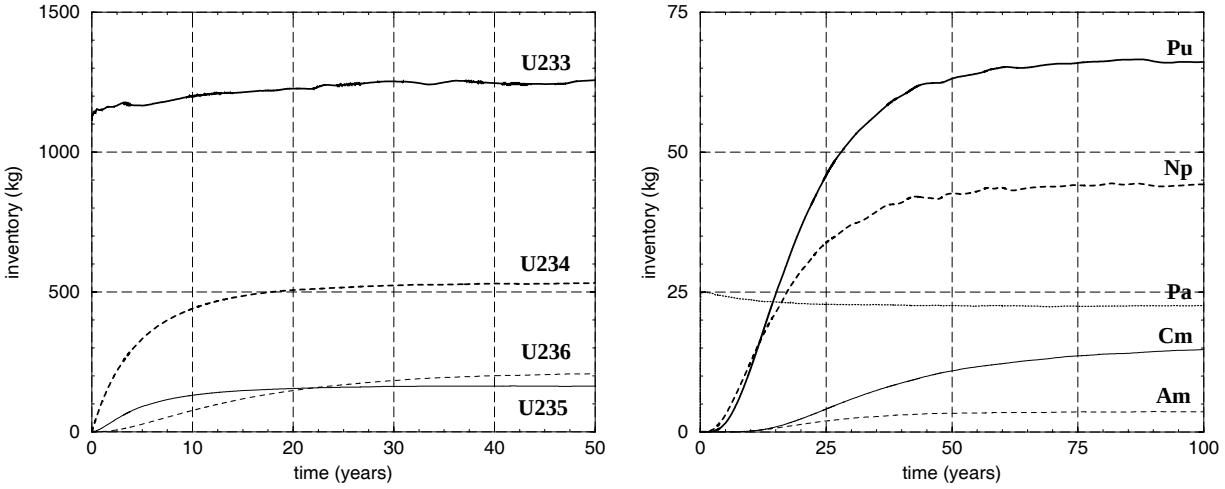

Figure 7: Evolution of the inventories of the main U isotopes and of other actinides in the fuel salt.

For actinides, transients are longer since less correlated to the short reprocessing time. The total actinide inventory is kept constant by regular thorium additions, allowing the fuel salt to remain chemically stable. The left part of Figure 7 shows the build-up of uranium isotopes from ^{233}U, whose slight fluctuations are due to the ^{233}U reinjection protocol based on our k_{eff} evaluation. Transients of other actinides are given element by element on the right part, with inventories more than 20 times lower than those of uranium. The Pa transient is linked to the reprocessing through its temporary storage and is thus very quick compared, for example, to Am and Cm transients which really begin only 10 years after start-up. Pa is composed essentially of ^{233}Pa, Pu of ^{238}Pu and Am of ^{243}Am.

4.3. Description of equilibrium

Equilibrium is reached after about one hundred years. This state is interesting as a point of comparison for further studies. Let us describe it in terms of neutron economy, waste production and, finally, temperature coefficients. Table 2 gives a global description of the neutron balance at equilibrium with detailed reactions in fuel salt, graphite and B_4C protections. Neutron production and consumption rates are normalized to one fission, and were all computed by MCNP with an accuracy of $\pm$ 10^{-3} n/fission. Subtracting the ^{233}Pa capture rate (0.006 n/f) from the ^{232}Th capture rate (1.030 n/f) gives the ^{233}U build-up rate (1.024 n/f). Dividing the latter by the ^{233}U total absorption rate (fission + capture = 0.987 n/f) then gives the breeding ratio (1.038), which amounts to a net ^{233}U production of 36 kg/y. The doubling time, necessary to breed an initial ^{233}U inventory of about 1.1 tons, is, thus, 31 y at equilibrium. As basic sensitivity studies, we performed a few evolution calculations with only one datum modified in each case. The most significant of them deals with the uncertainty on the ^{233}U α ratio of capture cross section over fission cross section, which is evaluated to $\pm$ 2.9% by the most recent integral evaluations available for an epithermal spectrum [15]. After taking this uncertainty into account over the entire transient, we obtained a breeding ratio of $1.038^{+0.006}_{-0.008}$ at equilibrium, which corresponds to a ^{233}U production of 36^{+6}_{-8} kg/y and a doubling time of 31^{+9}_{-4} y.

In addition to breeding performance, the neutron balance shows many other neutronic features of our reference system at equilibrium. Only ^{233}U and ^{235}U participate significantly to fissions, with respective contributions of 88% and 9%. The residual 3% are due to the other fissile nuclei, mainly ^{239}Pu, ^{241}Pu and ^{245}Cm. Such a partition of fissions determines a total proportion of delayed neutrons in the fuel salt of about 300 pcm. This value does not take into account the fraction lost in heat exchangers, which is evaluated to one third [9]. The effective proportion of delayed neutrons β_{eff} is thus about 200 pcm, which is low compared to a solid fuel U/Pu FBR with β_{eff} of about 350 pcm.

Reaction	**Production**	**Disappearance**	
fission	2.499	1.000	^{232}Th 0.007 **^{233}U 0.878** other U 0.094 Pu 0.019 Cm 0.002
$(n, 2n)$	0.026	0.013	^{9}Be 0.012 ^{232}Th 0.001
(n, γ)	-	1.412	^{7}Li 0.018 ^{9}Be 0.001 ^{19}F 0.012 FPs 0.015 **^{232}Th 1.030** ^{231}Pa 0.001 **^{233}Pa 0.006** **^{233}U 0.109** other U 0.158 ^{237}Np 0.021 Pu 0.037 Am 0.002 Cm 0.002
(n, α)	-	0.021	^{6}Li 0.004 ^{9}Be 0.004 ^{19}F 0.013
(n, p)	-	0.001	^{19}F 0.001
(n, γ) graphite	-	0.049	core 0.029 reflectors 0.020
(n, α) B_4C (^{10}B)	-	0.029	exchanger 0.028 vessel 0.001
leakage	-	0.000	-
total	2.525	2.525	-

Table 2: Detailed neutron balance (in n/fission) of the MSBR-like system at equilibrium.

The B_4C layer is thick enough to cancel leakage, which simplifies our k_{eff} evaluation. The graphite and B_4C total capture rate is about 5 times higher than the FP capture rate in the fuel salt, which illustrates the importance of FP extraction in the reference system. By detailing contributions element by element, we find that rare earths dominate, with almost 3/4 of FP captures in samarium (59%) and neodymium (14%). The light elements composing the fuel salt (Li, Be and F) absorb a bit less than graphite, since there are only traces of ^{6}Li and since ^{9}Be produces a few neutrons by (n,2n).

This neutronic description of equilibrium is completed by Table 3. The inventory of heavy nuclei is largely dominated by ^{232}Th with 65.6 t, for a total transuranic inventory of only 0.1 t. Let us point out some particular isotopes, important despite their low inventory. Because ^{233}Pa is extracted and temporarily stored out of flux, its inventory is only 21 kg in the fuel salt. This implies that about 80% of its decays take place in the storage tank, leading to a power of about 5.8 MW induced by the emission of the 570 keV gamma rays. An efficient cooling system would therefore be required, in this case. In comparison with a fast reactor, the ^{231}Pa inventory is low because of a lower production rate by (n,2n) on ^{232}Th and a larger capture rate in the MSR epithermal spectrum. The latter reaction is the main path for the production of ^{232}U, whose decay chain leads to the ^{208}Tl emitter of a 2.6 MeV gamma ray. The ^{232}U proportion of 0.1 mol% in uranium at equilibrium is quite sufficient to allow an easy detection of this gamma ray and, thus, to prevent ^{233}U proliferation from the fuel salt.

nucleus	$\sigma^{(n,\gamma)}$ (barn)	$\sigma^{fission}$ (barn)	inventory (kg)	nucleus	$\sigma^{(n,\gamma)}$ (barn)	$\sigma^{fission}$ (barn)	inventory (kg)
^{232}Th	1.50	0.0095	65560	^{241}Am	179	1.29	0.085
^{231}Pa	80.3	0.18	1.2	^{242}Am	21.4	192	0.0004
^{233}Pa	26.3	0.061	21.3	^{242m}Am	177	870	0.0015
^{232}U	14.8	19.4	2.8	^{243}Am	55.6	0.25	3.5
^{233}U	8.32	67.0	1250	^{242}Cm	5.2	0.39	0.07
^{234}U	20.5	0.27	530	^{243}Cm	12.4	118	0.0028
^{235}U	12.6	54.1	160	^{244}Cm	20.2	0.69	7.9
^{236}U	9.4	0.21	210	^{245}Cm	21.8	154	0.9
^{238}U	8.9	0.04	2.8	^{246}Cm	3.3	0.35	5.1
^{237}Np	45.4	0.24	44	^{247}Cm	21.1	31.8	0.3
^{239}Np	21.6	0.28	0.0026	^{248}Cm	9.0	0.55	0.8
^{238}Pu	37.1	2.27	49	^{249}Bk	580	3.4	0.01
^{239}Pu	112	184	6.3	^{249}Cf	55.4	210	0.003
^{240}Pu	256	0.34	2.9	^{250}Cf	540	0.50	0.01
^{241}Pu	59.8	166	3.2	^{251}Cf	280	610	0.008
^{242}Pu	39.7	0.21	4.9	^{252}Cf	3.2	6.5	0.06

Table 3: Mean capture and fission cross sections (in barn) and inventories (in kg) at MSBR equilibrium.

Our precise inventories allow us to know in detail the actinide waste production of the TMSR at equilibrium and to compare it with those of some other sustainable nuclear fuel cycles. We choose the radiotoxicity by ingestion as a criterion to evaluate the long-term potential radiological harmfulness of these wastes. The radiotoxicity R (in Sv) of nuclides i with inventories N_i and decay constants λ_i evolves as detailed in Formula 6. Dose coefficients r_i (in Sv/Bq) are given and regularly improved by the International Commission on Radiological Protection [16]. They depend on several parameters, among which the decay mode and the energy of the particles emitted.

$$R(t) = \sum_i r_i \ \lambda_i \ N_i(t) \tag{6}$$

Calculations of waste radiotoxicity R(t) are done using the code DECAY [17], which allows to solve the evolution system from disposal time up to 10^7 years later. The left part of Figure 8 shows the evolution of the waste radiotoxicity generated per GWth.y produced by several systems. Actinide wastes are clearly less radiotoxic with MSBR-like reference systems than with thorium-fueled FBRs, uranium-fueled FBRs and PWRs. At 10^3 years after discharge, once all short-lived FPs have decayed, MSR waste radiotoxicity is lower by respectively one, two and four orders of magnitude.

The right part of Figure 8 details element by element the contributions to the total evolving MSR waste radiotoxicity. Note that the daughters of a nuclide initially present at discharge are associated to its radiotoxic total contribution. We see that initial plutonium dominates actinide radiotoxicity up to one million years. If we look at isotopic contributions, we find that ^{238}Pu and ^{240}Pu dominate, except at about 10^5 years when the ^{233}U contribution rises because of its daughter ^{229}Th. Contrary to the case of the solid fuel Th/U FBR, this contribution does not really affect the total radiotoxicity since uranium losses are minimized thanks to the preliminary fluorination step.

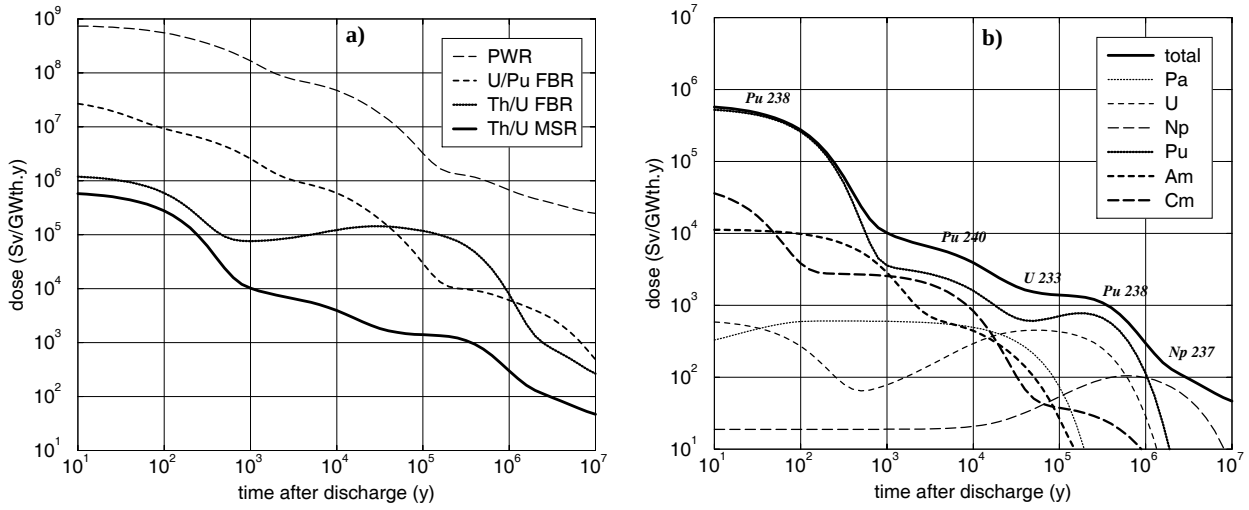

Figure 8: a) Radiotoxicity due to MSBR actinide wastes at equilibrium, compared to other fuel cycles [3]. MSBR actinide loss rate is 10^{-5} over $T_r = 10$ days. b) Contributions of elements to MSBR total waste radiotoxicity. Labels indicate the nuclei which contribute the most at a given time.

Let us finish this overview of wastes with two products that are more specific to MSR operation : tritium and graphite. Tritium is produced essentially by the ^{6}Li(n,t) and ^{7}Li(n,nt) reactions. Table 4 details tritium production during its quick transient and at equilibrium. Within the first 5 years, the ^{6}Li inventory is divided by 4 before stabilizing, whereas the ^{7}Li inventory and contribution to the tritium production rate are constant. At equilibrium, 150 g/y of tritium are produced, which is about 50 times higher than in a PWR, but half the production of a CANDU [18].

	$^6Li(n,t)$			$^7Li(n,nt)$		
	N (mol)	σ (barn)	rate (g/y)	N (mol)	σ (mbarn)	rate (g/y)
t = 0	81.9	111	292	1.64 10^6	1.77	93.4
t = 5 y	17.1	103	55.0	1.64 10^6	1.83	93.7
equilibrium	19.6	91.7	54.4	1.64 10^6	1.94	96.3

Table 4: Inventories N, cross sections σ and contributions to tritium production of ^{6}Li and ^{7}Li for the reference system, from start-up to equilibrium.

When graphite is irradiated, it tends to shrink first and then to expand quickly after a fast neutron fluence of about 10^{22} n/cm^2 above 50 keV. This defines a critical fluence F_{crit}, after which the graphite volume starts to increase indefinitely beyond its initial value. The time T_g associated to F_{crit} can thus be defined as the graphite lifetime. With the F_{crit} value of 3.0 10^{22} n/cm^2 considered by ORNL, we find $T_g = 6$ y as a mean value in the core whereas graphite in reflectors is not affected. This is consistent with the recommended 5-year period for graphite recycling in the MSBR project.

The last part of our description concerns safety and feedback coefficients, which quantify reactivity changes due to accidental temperature increases in the core. In practice, such an increase first occurs in the fuel salt, then propagates towards graphite with a delay of a few seconds at least. In the following, we evaluate these coefficients by taking the difference between the reference k_{eff} and the value given by another MCNP calculation simulating a situation of temperature increase. We distinguish different coefficients as given in Table 5, each of them corresponding to a modified MCNP description of the system. The Doppler coefficient is obtained by increasing the fuel temperature from 900 K up to 1200 K by means of the appropriate NJOY-computed data. The density coefficient corresponds to the fuel dilatation effect, and the salt coefficient takes the two latter effects into account. The graphite coefficient results from the influence of a temperature increase in the moderator on neutron diffusion, and the total coefficient combines it simultaneously with the salt effects.

	dilatation coefficient of salt ($g.cm^{-3}.K^{-1}$)	temperature coefficients (pcm/K)				
		Doppler	density	**salt**	graphite	**total**
thorium FLiBe MSBR-like t = 0	-6.7 10^{-4}	-3.5	+2.0	**-1.5**	+2.2	**+0.8**
thorium FLiBe MSBR-like equilibrium	-6.7 10^{-4}	-3.3	+2.6	**-1.0**	+1.6	**+0.7**

Table 5: Temperature coefficients of the re-evaluated MSBR at start-up and at equilibrium.

The Doppler broadening effect on the first ^{232}Th capture resonances at 20 eV explains its strongly negative coefficient. It is attenuated by salt dilatation, which increases reactivity by thermalization of the spectrum. The global salt effect remains negative and guarantees immediate safety. Because of the positive graphite effect due to a spectral shift propitious to ^{233}U fission (Figure 9), the total coefficient is positive. In the following, we test options that make the total coefficient negative.

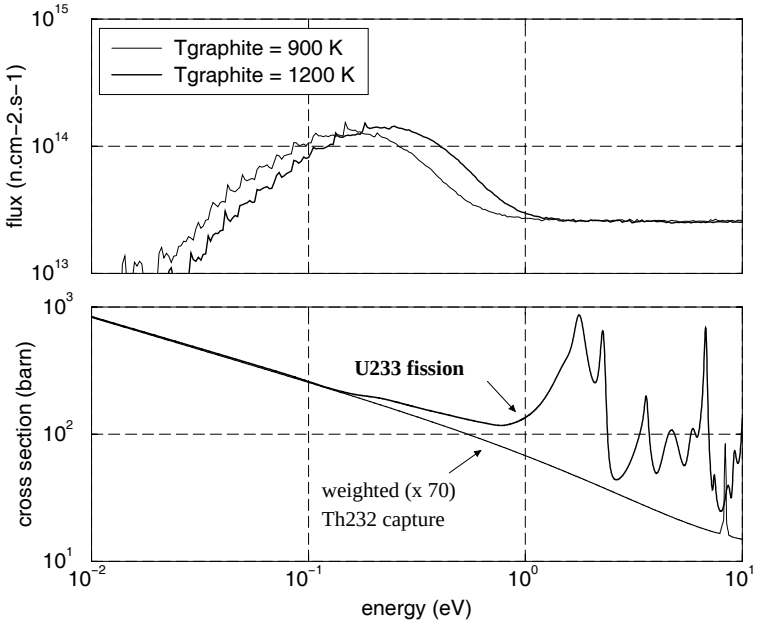

Figure 9: Average neutron spectra in MSBR core graphite for the temperatures $T_{graphite}$ of 900 K and 1200 K, and main cross sections (^{233}U fission and ^{232}Th capture) between 10^{-2} and 10^{1} eV.

4.4. Lessons from re-evaluating the MSBR project

This study of a reference system inspired from the MSBR project gives us a first complete view of the concept of Thorium Molten Salt Reactor. We verified that this reactor fulfills the three main requirements of economy, cleanliness and safety necessary to a sustainable nuclear energy production. By means of efficient pyrochemical reprocessing processes, FP and ^{233}Pa capture rates are limited to an extent which allows breeding, with a doubling time of 31 y at equilibrium. The low actinide inventory (2.2 t of uranium and 130 kg of transuranics at equilibrium) makes induced radiotoxicities the lowest among all the possible nuclear fuel cycles. Safety is the more delicate point, since only the instantaneous effect of salt heating on reactivity is negative. Nevertheless, this system is interesting enough to justify studying its practical start-up although no ^{233}U is available in nature.

5. POSSIBLE TRANSITIONS TO THORIUM CYCLE BASED ON THE REFERENCE MSBR

5.1. Transition based on Pu from fresh spent PWR fuel

We look into using another fissile isotope instead of ^{233}U to start the TMSR. We consider here in the reference FLiBe salt an initial inventory of "Pu UOX 5", which is extracted from the spent UOX fuel of a N4-type PWR after 5 years of cooling [19]. To reach criticality at start-up of this so-called Th/Pu UOX 5 $\rightarrow$ ^{233}U transition, we need about 4 tons of such plutonium. No additional plutonium is used after start-up. Figure 10 shows the replacement of Pu fissile isotopes by ^{233}U and ^{235}U in 10 years. The slight peaking of the ^{233}U inventory before it stabilizes to its equilibrium value allows maintaining criticality during the incineration of Minor Actinides (MAs), which takes about 20 y.

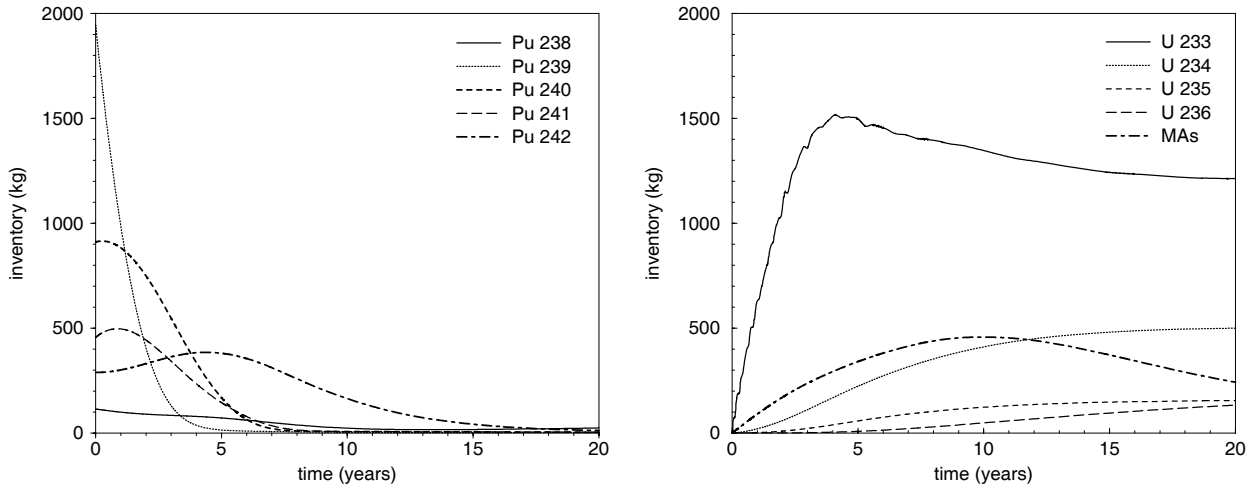

Figure 10: Evolution of plutonium and uranium inventories during the first 20 years of the Th/Pu UOX 5 $\rightarrow$ ^{233}U transition, at the reference power of 2500 MWth.

5.2. Sensitivity of the Th/Pu $\rightarrow$ ^{233}U transition to Pu type

If Pu is extracted from PWR fuel after a longer cooling time or a MOX recycling (compositions calculated from [19]), we find that its necessary inventory and then its incineration time increase significantly. As compared to the previous case, Table 6 shows that the Pu initial load is doubled with old Pu because of ^{241}Pu decay, and increases up to 18 t with ^{239}Pu-depleted MOX Pu. Figure 11 relates this to the spectrum hardening due to Pu captures, such as the ^{240}Pu resonance at 1 eV.

	UOX fuel, $T_c = 5$ y			UOX fuel, $T_c = 50$ y			MOX fuel, $T_c = 50$ y		
	σ_{cap}	σ_{fis}	N (kg)	σ_{cap}	σ_{fis}	N (kg)	σ_{cap}	σ_{fis}	N (kg)
^{238}Pu	13.7	1.78	110	9.3	1.70	190	6.4	1.63	620
^{239}Pu	24.4	42.0	1940	13.4	23.1	4630	8.2	14.1	7700
^{240}Pu	48.3	0.36	910	24.5	0.37	2200	10.5	0.39	6620
^{241}Pu	16.7	50.4	460	10.7	33.4	130	7.3	23.4	320
^{242}Pu	27.3	0.25	290	17.2	0.26	690	7.1	0.28	2620
total Pu	29.2	28.3	3710	16.7	14.4	7840	8.8	6.7	17880

Table 6: Mean cross sections (capture and fission, barn) and inventories (kg) of Pu isotopes at start-up of three Th/Pu → ^{233}U transitions, with effects of a longer cooling time T_c and MOX recycling.

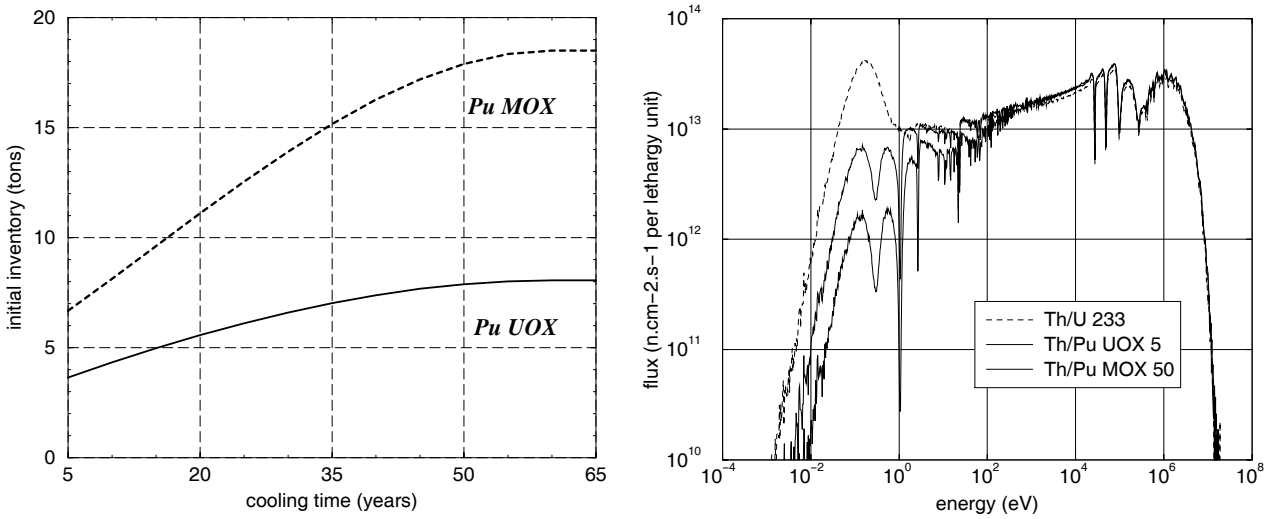

Figure 11: Initial inventories of plutonium and initial average neutron spectra in the salt at start-up of Th/Pu → ^{233}U transitions, depending on the type of used plutonium from PWR spent fuel.

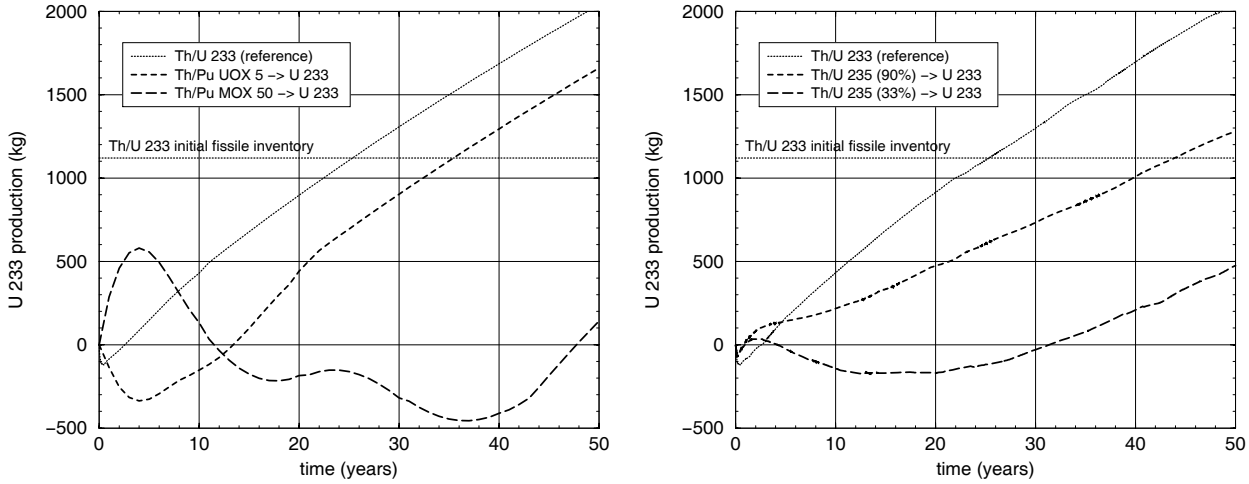

Figure 12: Comparison of ^{233}U productions in Th/Pu → ^{233}U and Th/^{enr}U → ^{233}U transitions.

The reference ^{232}Th/^{233}U equilibrium is reached by any Th/Pu $\rightarrow$ ^{233}U transition. In particular, the neutron spectrum softens until recovering its full thermal component. The initial Pu inventory delays the equilibrium, while it is being incinerated. This slows down ^{233}U total production, as shown in the left part of Figure 12 for the Th/Pu $\rightarrow$ ^{233}U transitions in comparison with the reference ^{232}Th/^{233}U transition. In the latter case, the so-called first doubling time necessary to produce an initial ^{233}U inventory of 1.1 t after start-up is 25 y, whereas it is delayed to 35 y with Pu UOX 5 and to 70 y with Pu MOX 50. The right part of Figure 12 shows two similar transitions based on ^{235}U-enriched uranium instead of Pu. Uranium at 90% ^{235}U is a bit less efficient than Pu UOX 5 because of ^{236}U poisoning, whereas the incineration of ^{238}U is too long with 33% of ^{235}U.

5.3. Transition scenarios depending on deployment needs

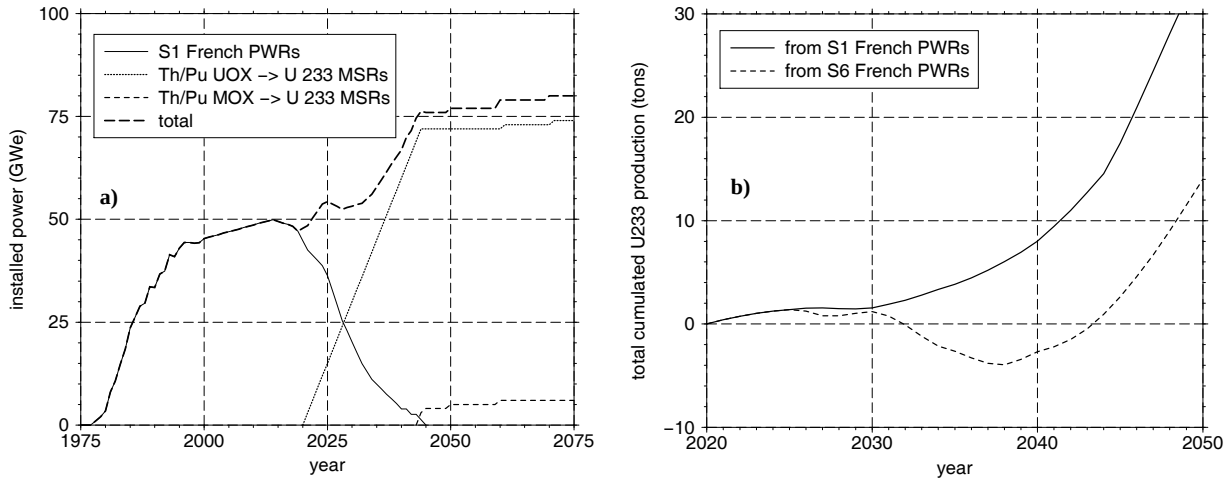

Figure 13: a) Th/Pu $\rightarrow$ ^{233}U transition from S1 PWRs (no MOX after 2010), with total incineration of Pu. b) ^{233}U stock in this scenario, compared to transition from S6 PWRs (MOX until the end).

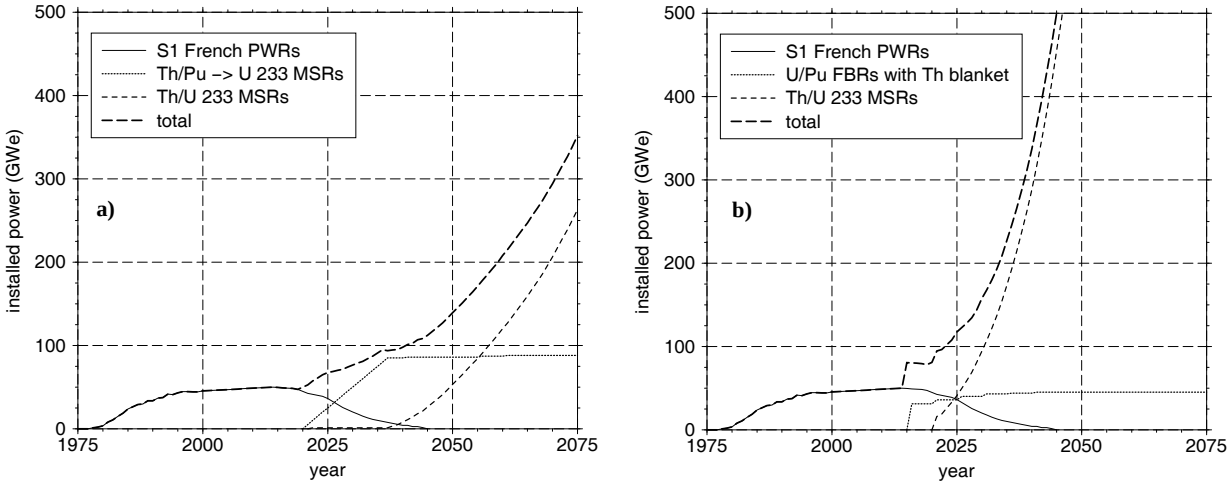

Figure 14: a) Deployment scenario based on the optimal use of PWR Pu in Th/Pu $\rightarrow$ ^{233}U MSRs and the start-up of Th/^{233}U reference MSRs. b) "PWRs-FBRs-MSRs" scenario based on the use of PWR Pu in U/Pu FBRs which produce ^{233}U in their thorium blankets for Th/^{233}U reference MSRs.

We consider scenarios based on the Th/Pu $\rightarrow$ ^{233}U transition, at a constant installed power and then with a maximal deployment. As a world representative situation, we choose the present French PWRs. For a precise description of the Pu available, we distinguish two evolutions, based on the stopping (S1 scenario) or the continuation (S6 scenario) of MOX recycling [20]. Figure 13 shows that starting the Th/Pu $\rightarrow$ ^{233}U reactors in 2020 allows consumption of the entire stock of plutonium with a power increase of about 50%. Once Th/Pu $\rightarrow$ ^{233}U transitions are effective, the reactors operate at the ^{232}Th/^{233}U equilibrium and breed ^{233}U, giving ^{233}U stock evolutions shown in the right part of Figure 13. This proves that stopping MOX recycling would ease this scenario.

In our maximal deployment scenarios of Figure 14, the ^{233}U stock is rather used to start as many TMSRs as possible. Scenario a) can only reach a factor 3 on the installed power by 2050. Scenario b) replaces the slow Th/Pu $\rightarrow$ ^{233}U transition by fast U/Pu isogenerators started in 2015 and breeding ^{233}U in thorium blankets at the rate of 200 kg/y. A factor 12 is then obtained by 2050, fulfilling the factor 10 considered in the intensive nuclear hypothesis of the introduction.

5.4. Impact of deployment results on our system studies

The thermal spectrum of the reactor makes most of the Th/Pu $\rightarrow$ ^{233}U transitions difficult, with a transient transuranic inventory which can cause solubility or reprocessing problems. Moreover, our scenarios of significant deployment show that an upstream ^{233}U production in a few classical reactors allows a quicker start of TMSRs directly with ^{233}U than the Th/Pu $\rightarrow$ ^{233}U way. These statements lead us to focus now on the study of TMSR operation with ^{232}Th/^{233}U fuel from the start.

6. EXPLORATION OF ALTERNATIVES TO MSBR OPTIONS FOR ENERGY PRODUCTION

6.1. Optimization of core neutronics

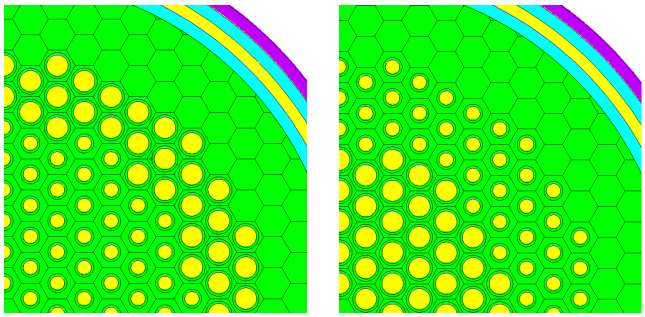

Figure 15: Core with fertile zone at the edge (left) and core with fertile zone at the center (right).

The aim here is to show to which extent neutron balance can be improved for breeding through two significant examples of core modifications. The first one deals with the channel size, that is to say with the volumic proportion of salt in graphite. For easier comparison with the single zone reference core, we study only two options, shown in Figure 15, for the layout of two zones within the core while unchanging the total salt volume. The zone with a smaller channel diameter (12 cm, 19.4 vol% of salt) is more moderated than in the reference case, whereas the one with a bigger channel diameter (18 cm, 43.5 vol% of salt) is less moderated. We choose to call the latter the "fertile zone" since it should advantage ^{232}Th capture in the epithermal part of the spectrum against ^{233}U fission. Evolution calculations of both configurations up to equilibrium show that a fertile zone placed at the edge makes the system breed better, whereas breeding is inhibited when it is placed at the center.

By detailing zone contributions to the breeding ratio in each case, Table 7 confirms that a fertile zone at the edge improves breeding. In this case, we see an interesting specialization between the central zone where ^{233}U is especially used up by fission and the fertile zone where ^{232}Th is especially used up by capture. A drawback of this configuration is that the radiation damage rate in the graphite at the center is 50% larger than in the reference core, reducing the graphite lifetime to the same extent. In terms of safety, the global salt and total temperature coefficients are unchanged with this option compared to the reference, whereas they are better with a fertile zone at the center (respectively -1.6 and -1.1 pcm/K) since the salt contribution is then increased against that of graphite.

	internal zone		external zone		rest of circuit		τ_b of full
	a_{u3} (%)	τ_b	a_{u3} (%)	τ_b	a_{u3} (%)	τ_b	circuit
single zone (reference)	66.2	**1.026**	32.6	1.006	1.2	2.500	**1.038**
fertile zone at the edge	75.5	0.980	22.4	**1.267**	2.1	1.286	**1.051**
fertile zone at the center	34.0	1.170	63.3	0.851	2.7	1.852	**0.987**

Table 7: Proportion a_{u3} of absorptions in ^{233}U and breeding ratios τ_b zone per zone, for the three core configurations (reference, external and internal fertile zone).

Another option is to replace the FLiBe salt by FLiNa, whose molar composition is 54.5% LiF - 13.5% NaF - 32% ThF_4 for a melting point of 525 ^{o}C and a density of 3.3 g/cm^3 at 900 K. We compute the evolution of this salt in our reference geometry in order to compare it with FLiBe. Parasitic captures in light salt components are slightly lower with FLiNa, but the heavy nuclei inventory is higher because of the salt composition. This leads to a higher inventory of ^{233}U (1.76 t) and transuranics (190 kg) at equilibrium, and to a longer doubling time (39 y). In the case of FLiBe, part of ^{6}Li is regenerated by the ^{9}Be(n,α) reaction. With FLiNa, this regeneration is no longer possible and ^{6}Li remains only as traces, with 0.06 mol instead of 19.6 with FLiBe. Then, only the ^{7}Li(n,nt) reaction contributes to tritium production. Since the LiF proportion is lower than in FLiBe, the tritium production rate at equilibrium is close to 50 g/y, that is to say about one third of the value obtained with FLiBe. For Table 8, we estimate a range for the FLiNa dilatation coefficient. We find that the salt temperature coefficient is better, giving a smaller positive total coefficient. It could even be slightly negative if the more favorable hypothesis were supported by measurements.

	dilatation coefficient	temperature coefficients (pcm/K)				
	of salt (g.cm^{-3}.K^{-1})	Doppler	density	**salt**	graphite	**total**
thorium FLiNa	-5.0 10^{-4}		+1.6	**-2.0**		**+0.4**
MSBR-like		-3.4			+2.1	
t = 0	-1.0 10^{-4}		+0.4	**-3.2**		**-0.8**
thorium FLiNa	-5.0 10^{-4}		+1.9	**-1.7**		**0.0**
MSBR-like		-3.7			+1.5	
equilibrium	-1.0 10^{-4}		+0.5	**-3.3**		**-1.9**

Table 8: Temperature coefficients of the re-evaluated MSBR at start-up and at equilibrium with FLiNa instead of FLiBe, with two framing values for the poorly known FLiNa dilatation coefficient.

6.2. Flexibility of pyrochemical reprocessing

The reference reprocessing allows easy breeding, but may seem somewhat too ambitious. We try here to evaluate the latitude we have on reprocessing by testing modified versions. Table 9 compares the changes in the neutron balance at equilibrium between the reference and two such versions.

	nuclei	reference		T_r = 30 days		Pa reinjection	
		τ (n/f)	σ (barn)	τ (n/f)	σ (barn)	τ (n/f)	σ (barn)
fission	^{232}Th	0.007	0.0095	=	0.0096	=	0.0097
	^{233}**U**	**0.878**	67.0	**0.872**	64.6	**0.861**	63.4
	other U	0.094	9.8	0.099	9.5	0.109	9.3
	trans-U	0.021	15.6	0.022	15.1	0.023	14.7
(n,γ)	Li + Be + F	0.031	0.0022	0.027	0.0021	0.028	0.0021
	FPs	0.015	3.19	0.029	2.18	=	3.49
	^{232}**Th**	**1.030**	1.50	**1.002**	1.48	**0.982**	1.47
	^{231}Pa	0.001	80.3	=	78.2	=	76.8
	^{233}**Pa**	**0.006**	26.3	**0.012**	25.7	**0.025**	25.2
	^{233}**U**	**0.109**	8.32	**=**	8.08	**0.108**	7.93
	other U	0.158	16.5	0.166	15.9	0.181	15.4
	trans-U	0.062	47.4	0.066	45.8	0.072	44.9

Table 9: Fission and capture reaction rates τ and mean cross sections σ at equilibrium for reference, T_r = 30 days and T_r = 10 days with no Pa decay outside. "=" means "same value as reference".

Increasing the reprocessing time to 30 days makes FP and Pa capture more. At equilibrium, FPs have their inventory about 3 times larger (610 kg) but capture only twice as much, because of a slight hardening of the spectrum shown by Table 9 mean cross section values. The Sm contribution decreases to 44% of FP captures, whereas Nd increases to 21%. The ^{233}Pa inventory and its capture rate are only doubled, due to additionnal β^- decays. Overall extra uranium and transuranic inventories are respectively 160 kg and 10 kg. The breeding ratio is reduced to 1.009 at equilibrium. The last column of Table 9 concerns the equilibrium obtained with the reference reprocessing time T_r but immediate Pa re-injection, which prevents ^{233}U proliferation from the decay tank. The ^{233}Pa inventory is then multiplied by 5 as compared to the reference equilibrium value of about 20 kg. This leads to an additional inventory of 80 kg for ^{233}U, 150 kg for ^{234}U, 40 kg for ^{235}U, 60 kg for ^{236}U and 30 kg for transuranics. The breeding ratio is reduced to 0.988, which amounts to a ^{233}U consumption rate of 11 kg/y. The protactinium effect remains manageable by a single central control rod, with a reactivity increase associated to a 27-day power stop of 1600 pcm instead of 500 pcm in the reference case.

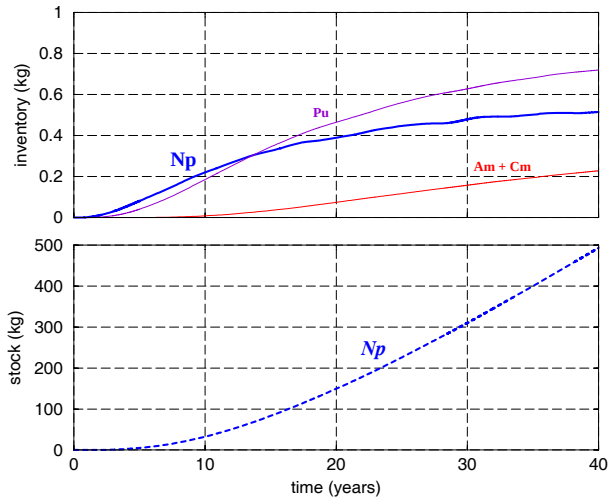

Figure 16: Transuranic inventories and stocks when Np is extracted.

Together with uranium, neptunium is extracted as a volatile hexafluoride at fluorination. Instead of being reinjected into the fuel salt after reduction by H_2, NpF_6 can be isolated at more than 99% by absorption on NaF heated from 200 to 400 ^{o}C [21]. Figure 16 shows that this reduces the transuranic inventory to about 2 kg, for a Np accumulation rate of 20 kg/y. This rate is equal to the Np reference capture rate, which explains that uranium inventories and reaction rates are almost not modified. Figure 17 details how Np extraction short-circuits Pu production. Two thirds of the additional neutrons made available lead to ^{232}Th captures, increasing the breeding ratio up to 1.058 at equilibrium. This amounts to a ^{233}U production of 56 kg/y and a doubling time of 20 y. The actinide waste radiotoxicity is a bit higher, but remains between 10^4 and 10^5 Sv/GWth.y after discharge.

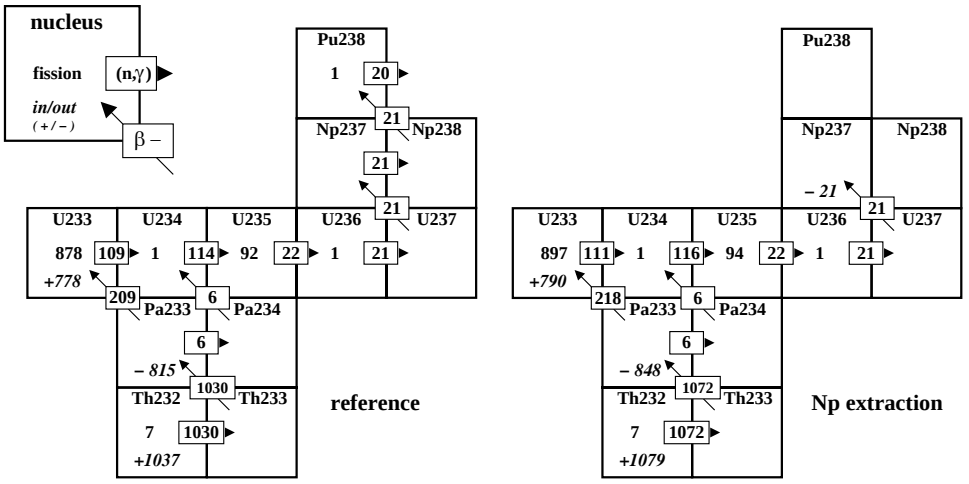

Figure 17: Representation in the (N,Z) plane of the reference equilibrium, compared to the one obtained with Np extraction. Decay and reaction rates are normalized to 1000 fissions.

6.3. Insertion of neutron absorbing pins into the core

We first consider here ^{129}I (half-life of 1.6 10^7 y) and ^{99}Tc (half-life of 2.1 10^5 y) transmutation in the TMSR. Contrary to the reference reprocessing, we recycle iodine in the salt in order to transmute ^{129}I at its production rate of 10.2 kg/y into stable volatile ^{130}Xe, for an inventory of 290 kg. We add 2.5 cm-diameter graphite pins at the edge of the core as described in the left part of Figure 18. We determine in these pins an optimal Tc concentration of 2 mol%, so that ^{99}Tc is transmuted at its production rate of 18.0 kg/y over 5 years into stable ^{100}Ru, for an initial inventory of 400 kg.

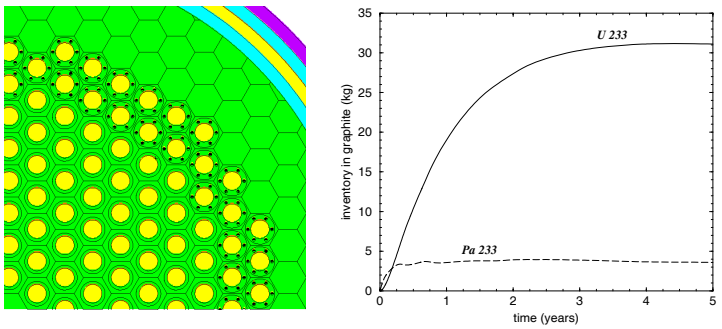

Figure 18: Reference core with graphite pins around channels at the edge for ^{99}Tc transmutation or ^{233}U production. Evolution of ^{233}Pa and ^{233}U inventories (kg) in graphite pins for the latter case.

The breeding ratio is about 0.99 in these conditions of ^{129}I and ^{99}Tc transmutation. Both salt and graphite temperature coefficients are improved thanks to the respective ^{129}I and ^{99}Tc Doppler effects, and the total coefficient is close to zero. This option allows thus the improvement of temperature coefficients in addition to long-lived FP transmutation. A method replacing ^{99}Tc by the neutronic poison ^{167}Er has been studied by EDF [22]. A negative total coefficient can then be obtained, but the pin reprocessing frequency is higher because of the high value of ^{167}Er capture cross section.

Another interesting possibility is to use ^{232}Th. While recycling iodine, we replace then ^{99}Tc by 6 mol% of ^{232}Th in the same graphite pins as shown in Figure 18, which gives us a breeding ratio of 1.00. The right part of Figure 18 shows that this way of breeding gives a doubling time of about 60 y over one-year cycles. The temperature coefficients are the same as with ^{99}Tc. The difference is that, in this case, the improvement of the temperature coefficients is compatible with breeding, provided that ^{233}U is recovered efficiently. ^{232}Th could be placed in reflectors too, e.g. in a fluoride salt.

6.4. Evolution of the TMSR concept towards reprocessing simplification

Breeding had priority in the MSBR studies, leading to ambitious reprocessing options and barely acceptable temperature coefficients. These two main drawbacks clearly prevent this system from being a competitive Generation IV energy producer. However, we find, in Section 5, that breeding constraints can be reduced thanks to upstream ^{233}U production, giving a great deal of latitude to simplify the reprocessing and improve the safety. Most of the options studied here improve either feasibility (slowing down reprocessing, giving up Pa extraction) or safety (FLiNa fuel salt, poison pins), while lowering the neutron breeding margin. A synthesis of such possible options is underway, for a complete TMSR proposal. With this goal in view, a recent study proposes a drastic reprocessing simplification based on thorium precipitation [23]. It also shows how lowering the volumic power can improve the neutron economy, especially by reducing neutron leakage and ^{233}Pa capture rate.

7. CONCLUSIONS

Our work, partly described in this paper, emphasizes the great advantages of the MSR concept applied to energy production with thorium. The studies performed at ORNL in the sixties led us to explore this system further under the hypothesis of a significant contribution of nuclear energy to the world supply in the coming decades. By means of computing tools developed around the Monte Carlo MCNP code, we first re-evaluated from start up to equilibrium a reference system inspired by the historical MSBR. Taking into account the efficient lanthanide extraction, we checked good breeding performance with a breeding ratio of about 1.04 at equilibrium. The very low actinide inventory (2.3 t) allows to reduce waste radiotoxicity, by more than two orders of magnitude at 1000 y after discharge as compared to the fast uranium cycle. The constraint of intrinsic safety is barely respected by our MSBR-like reference system, at least instantaneously, thanks to a negative salt coefficient.

These interesting features for a sustainable nuclear energy production led us to study how such a reactor could be started, with no ^{233}U available in nature. We found that transition to the asymptotic ^{232}Th/^{233}U cycle is possible using an initial Pu inventory extracted from PWR spent fuel, provided that its fissile quality is good enough. Such a Th/Pu $\rightarrow$ ^{233}U transition seems nevertheless quite difficult, extending over decades and jeopardizing the feasibility of the reprocessing processes. Alternatively, we demonstrate the efficiency of a symbiotic scenario based on TMSRs and a few complementary self-regenerating U/Pu FBRs, producing ^{233}U in thorium blankets. The start-up of TMSRs directly in a ^{232}Th/^{233}U regenerating mode, close to equilibrium, thus seems highly preferable.

These deployment results spurred us then on core geometry and reprocessing optimizations for operation with Th/^{233}U fuel from the start. Such an exploration aimed at finding ways to improve the neutron economy, not only for breeding but for concept simplification and safety too. A fertile zone at the edge of the core increases the breeding ratio up to 1.05 by optimizing the location of ^{232}Th captures and ^{233}U fissions. Replacing FLiBe by FLiNa reduces tritium production by a factor of 3, and tends to make the total temperature coefficient negative. The neutron balance can be adjusted by fuel reprocessing, e.g. by slowing down FP extraction, by suppressing Pa outer decay or by extracting Np. All these examples illustrate the great flexibility of the TMSR concept, and should be combined into a simpler and safer system, which would (barely) regenerate its own ^{233}U.

Our present studies deal precisely on one hand with specifying a simplified TMSR in view of a large nuclear energy production, on the other hand with initial ^{233}U production in solid fuel reactors such as FBRs or PWRs. Only a significant simplification of the TMSR concept can lead to a really competitive Generation IV energy producer. This implies alternative, less stringent, reprocessing options, maintaining only essential steps such as uranium fluorination and helium bubbling, which make both the fissile inventory and the reactivity reserve very low. In order to keep the system regenerating under these new reprocessing conditions while improving temperature coefficients, some core parameters like the flux level have to be optimized as well. Let us note that decreasing the flux is all the more interesting as it could increase the graphite lifetime by the same ratio. Such a necessary concept simplification rests on the possibility to produce ^{233}U in more classical solid fuel reactors using plutonium recovered from spent PWR fuel. For this reason, the future studies on the TMSR can and should be closely linked to R&D on other reactors, such as gas-cooled fast or thermal reactors, and to complete studies of deployment scenarios based on complementary systems.

Acknowledgements

One of the authors (A.N.) acknowledges partial support from D. Lecarpentier, C. Garzenne and J. Vergnes from EDF, Clamart. For their help on molten salts and pyrochemistry, we are grateful to M. Allibert, P. Faugeras and the other specialists met within french GEDEON workshops and european MOST meetings. We thank E. Huffer and D. Kerdraon for their valuable editing.

References

1. IIASA-WEC (1998), Global Energy Perspectives, Cambridge University Press, London.

2. H. Nifenecker, O. Méplan and S. David (2003), Accelerator Driven Subcritical Reactors, Institute of Physics Publishing.

3. S. David et al (2000), Fast Subcritical Hybrid Reactors for Energy Production : Evolution of Physical Parameters and Induced Radiotoxicities, Nucl. Instr. and Meth. A 443, 510-530.

4. A. Nuttin et al (2001), Thorium Fuel Cycles : a Graphite-Moderated Molten Salt Reactor versus a Fast Spectrum Solid Fuel System, GLOBAL 2001, Paris, France, 9-13 September.

5. P. N. Haubenreich et al (1970), Experience with the Molten Salt Reactor Experiment, Nucl. App. and Tech. 8, 118-136.

6. E. S. Bettis et al (1970), The Design and Performance Features of a Single-Fluid Molten-Salt Breeder Reactor, Nucl. App. and Tech. 8, 190-207.

7. Groupe de travail CEA-EDF "cœur" (1983), Synthèse des études réalisées entre 1973 et 1983, dossier "cœur", EDF Report HT/12/75/83.

8. K. Furukawa et al (1990), Thorium Molten-Salt Nuclear Energy Synergetics, Journal of Nuclear Science and Technology 27, 12, 1157-1178.

9. D. Lecarpentier and J. Vergnes (2002), The AMSTER (Actinide Molten Salt TransmutER) Concept, Nucl. Eng. and Des. 216, 43-67.

10. A. Nuttin (2002), Potentialités du concept de réacteur à sels fondus pour une production durable d'énergie nucléaire basée sur le cycle thorium en spectre épithermique, Grenoble I, thesis.

11. Generation IV International Forum (2002), A Technology Roadmap for Generation IV Nuclear Energy Systems, Report GIF-002-00.

12. M. E. Whatley et al (1970), Engineering Development of the MSBR Fuel Recycle, Nucl. App. and Tech. 8, 170-178.

13. J. F. Briesmeister (1997), MCNP4B - A General Monte Carlo N Particle Transport Code, Los Alamos Laboratory Report LA-12625-M.

14. R. E. MacFarlane (1998), NJOY97 - Code System for Producing Pointwise and Multigroup Neutron and Photon Cross Sections from ENDF/B-VI Data, RSICC Code Package PSR-368.

15. A. M. Perry (1968), Influence of Neutron Data in the Design of Other Types of Power Reactors, Conference on Neutron Cross Sections and Technology, Washington DC, USA, 4-7 March.

16. International Commission on Radiological Protection (1995), Compilation of Ingestion and Inhalation Dose Coefficients, Publication 76.

17. S. Ménard and J.-P. Schapira (1995), Impact radiologique à long terme de l'extraction du thorium, Institut de Physique Nucléaire d'Orsay, Report DRE 95-07.

18. R. B. Briggs (1971), Tritium in Molten Salt Reactors, Reactor Technology 14, 4, 335-342.

19. S. Sala (1995), Réduction de la radiotoxicité des déchets nucléaires, Aix-Marseille I, thesis.

20. P. Girard, Y. Marignac and J. Tassart (2000), Le parc nucléaire actuel, Mission d'évaluation de la filière nucléaire, France.

21. M. Jacquin, A. Lecocq and J.-L. Romet (1976), Traitement en continu du sel MSBR, EDF Report HF/13/11/76.

22. D. Lecarpentier et al (2003), Temperature Feedbacks of a Thermal Molten Salt Reactor : Compromise between Stability and Breeding Performance, ICAPP'03, Córdoba, Spain, 4-7 May.

23. L. Mathieu et al (2003), Thorium Molten Salt Reactor : from High Breeding to Simplified Reprocessing, GLOBAL 2003, New-Orleans, USA, 16-20 November.